Research on Thermal Calculation and End Winding Heat Conduction Optimization of Low Speed High Torque Permanent Magnet Synchronous Motor

Shengnan Wu, *Member*, *IEEE*, Zhimin Li, and Wenming Tong, *Member*, *IEEE*

***Abstract*—Because of its simple structure, large torque and high efficiency, permanent magnet synchronous motor of low speed and high torque is widely adopted in many fields. In this paper, a 394.5kW mining low-speed high-torque permanent magnet synchronous motor (LSHTPMSM) is regarded as the study object. According to the physical model, a three-dimensional equivalent heat transfer temperature field calculation model of the motor is built to simulate the temperature distribution of the motor under rated conditions. In terms of the serious issue of stator winding temperature increase of permanent magnet synchronous motor of low speed and high torque, the heat conduction optimization of the end of the stator winding is studied, which enhances the heat dissipation effect of the stator end winding, effectively reduces its temperature increase and temperature gradient with the winding in the slot, and improves the practical efficiency and service life of the motor. Finally, the motor temperature rise test platform is constructed for the verification of the feasibility of the optimization scheme, which provides a reference direction for the heat dissipation optimization of permanent magnet synchronous motor of low speed and high torque.**

***Index Terms*—Permanent magnet synchronous motor, Temperature field, Thermal optimization.**

I. INTRODUCTION

WITH the rapid progress of science and technology and the rapid development of society, permanent magnet synchronous motor of low speed and high torque have also developed rapidly. Not only the stability and various performance indicators have been greatly improved, but also the volume has been reduced compared with traditional motors. At the same time, it reduces the noise emitted during operation, so it has been widely developed in the mining field [1]. Due to the high temperature rise during the normal operation of the permanent magnet synchronous motor of low speed and high torque and the limited heat dissipation conditions, the insulation will be burned in the long-term operating environment, which will affect the normal and stable operation of the motor and the service life of the motor. Hence, the study of the heat dissipation of the motor becomes very important.

Currently, there are three major approaches for motor thermal calculation: equivalent thermal network approach, finite element approach and finite volume approach. In References [2]-[3], the thermal discussion on the motor was made by the equivalent thermal network approach, and the validity of the results was validated by tests, which improved the calculation speed of the motor temperature increase. In References [4]-[7], the temperature increase of different motors under extreme overload operation was studied by finite element approach, and the precision of the results was greatly improved by experiments. In reference [8]-[12], the fluid field and temperature field of the motor are calculated by the finite volume approach, and the flow state of the air inside the motor and the distribution of the temperature increase of the motor are obtained. The state parameters of various cooling media under different cooling methods are compared, and the results are proved by experiments. The cooling capacity of the motor is improved, which is beneficial to the long-time steady operation of the motor.

Different thermal calculation methods have their own advantages. The model of the equal thermal network approach is simple and the calculation speed is fast, but only the overall temperature rise distribution can be obtained. The finite volume approach can calculate the heat dissipation parameter of different coupling boundaries and obtain the overheated part, but it has high requirements for computer configuration and large calculation cost. The finite element approach can calculate the position of the motor's hot spot and better simulate the working conditions in the real environment, so it is widely used.

At present, most of the LSHTPMSM use water-cooled cooling methods, which will greatly reduce the temperature rise in the axial middle position of the stator winding, but it will also cause a higher temperature rise at the end of the winding. In this paper, a 394.5kW mining LSHTPMSM is regarded as the study object. Firstly, a three-dimensional equivalent heat transfer

Manuscript received February 08, 2023; revised March 28, 2023; accepted May 08, 2023. Date of publication December 25, 2023 Date of current version July 21, 2023.

This work was supported by the National Natural Science Funds of China No. 51907129 and Technology program of Liaoning province No. 2021-MS-236. (*Corresponding Author*: *Wenming Tong*)

Shengnan Wu, Zhimin Li and Wenming Tong are with the School of Electrical Engineering, Shenyang University of Technology, Shengyang 110870, China (e-mail: imwushengnan@163.com; 1115913268@qq.com; twm822@126.com).

Digital Object Identifier 10.30941/CESTEMS.2023.00039

model of the motor is built according to the physical model. Because the winding in the stator core slot is the main heat source, it is the biggest influencing factor of the temperature increase of the motor. Then, the thermal simulation of the motor under rated operating condition is carried out by finite element approach. At the same time, the temperature increase test platform of the motor is built to verify the correctness of the simulation results. Finally, the problem of high temperature increase of the stator core winding of the motor is optimized and analyzed, which efficiently decreases the temperature increase of the winding and the temperature gradient between the end winding and the slot winding. The feasibility of the optimization scheme is proved by the prototype experiment, which offers a reference direction for the heat dissipation optimization of this kind of the permanent magnet synchronous motor of low speed and high torque.

II. Establishment of Motor Heat Transfer Model

A. Motor Parameters and Structure

Table I shows the major coefficients of the motor herein. Fig. 1 shows the three-dimensional physical model of the motor based on the main parameters and cooling structure of the motor. The motor in this research uses the cooling structure of casing water cooling. The heat produced by the stator group is mainly transmitted to the stator core along the radial direction to the casing, which is absorbed by the circumferential cooling water channel embedded in the casing to cool the motor.

TABLE I
MAIN PARAMETERS OF MOTOR

Parameter	Value
Rated power(kW)	394.5
Outside diameter of stator(mm)	1400
Rated voltage(V)	1140
Air gap length(mm)	2.8
Rated speed(r·min^{-1})	50
Number of poles	60
Number of stator slots	72

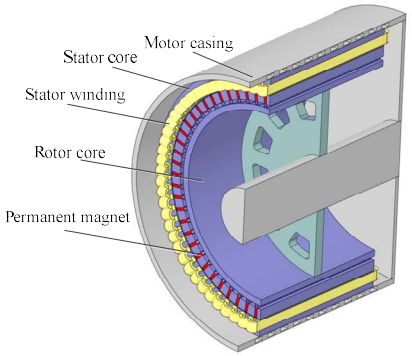

Fig. 1. Three-dimensional equivalent heat transfer model of motor.

B. Fundamental Assumption

For convenient calculation, the motor stator winding part is assumed as follows:

1) The two sides of the windings in the stator slot are exactly the same, and the heat generation is the same;

2) Regardless of different insulating materials in the tank, various insulation and air in the tank are equal to an insulating entity with the same thermal conductivity;

3) It is assumed that the external insulation of the copper wire in the stator winding of the motor is evenly distributed and closely contacts the stator core without gap;

4) The winding end is equivalently processed according to the actual model;

5) The thermal conductivity of every material of the motor does not change with time.

According to the above assumptions, Fig. 2 shows the equivalent entity in the stator core slot.

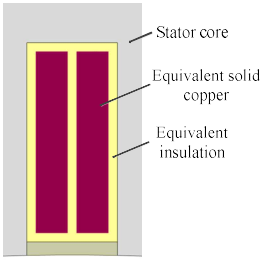

Fig. 2. Equivalent model of motor stator core winding.

According to the principle of heat dissipation, the basic thermal parameters of the equivalent entity in the stator slot can be obtained: thermal conductivity, density and specific heat capacity, as shown in Formulas (1) and (2) [13].

$$\lambda = \frac{d_1 + d_2 + \cdots + d_i}{\frac{d_1}{\lambda_1} + \frac{d_2}{\lambda_2} + \cdots + \frac{d_i}{\lambda_i}} \tag{1}$$

$$\begin{cases} \rho = \dfrac{\rho_1 V_1 + \rho_2 V_2 + \cdots + \rho_i V_i}{V} \\ c = \dfrac{c_1 \rho_1 V_1 + c_2 \rho_2 V_2 + \cdots + c_i \rho_i V_i}{\rho V} \end{cases} \tag{2}$$

where: λ is the equivalent thermal conductivity; ρ is the bulk density; c is the specific heat capacity; V is the volume; d_1, d_2, $\cdots$, d_i are the thickness of the thermal conductor.

C. Boundary Condition

According to the stable operation performance of the motor under rated situation and the characteristics of its cooling structure, the border conditions are shown below:

1) The circumferential inlet of the channel is regarded as the boundary condition of the velocity inlet, and the velocity of the inlet is 0.2m/s. The outlet of the circumferential waterway is set as the boundary of the pressure outlet, and the temperature of the environment is set to the limit working temperature of 40 °C;

2) The contact surface between the rotor core and the air gap is set as a rotating wall surface, and the rotational speed is set to the rated rotational speed of 50 r/min.

The motor usually includes two boundary conditions during thermal calculation: heat dissipation boundary and adiabatic boundary. At the symmetric boundary of the model is the adiabatic boundary; the heat dissipation boundary changes according to different cooling methods of the motor, and the convection heat dissipation parameter of different parts in contact with the cooling medium in the motor is calculated by

the flow velocity of different cooling media.

The selection of the surface heat dissipation coefficient formula needs to be as reasonable as possible according to the actual situation of the motor. Because the internal space of the motor studied herein is closed and the rated speed of the motor is low, the heat dissipation parameter of the stator core and rotor surface of the motor is obtained according to the empirical formula[13], and the results are shown in Table II.

$$\begin{cases} \alpha_s = \dfrac{1+0.25v_s}{0.045} \\ \alpha_r = 28\left(1+\sqrt{0.45v_r}\right) \end{cases} \tag{3}$$

TABLE II
HEAT DISSIPATION PARAMETER OF EACH SURFACE OF MOTOR

Heat dispersing surface	Coefficient of heat emission($W\cdot m^{-1}\cdot K^{-1}$)
End surface of stator core	22.2
End surface of rotor core	28

The motor speed in this paper is low, and a simple air gap equal thermal conductivity method is adopted for analyzing the temperature rise. The air gap equal thermal conductivity is not only related to the structural factors of the motor, but also to the thermal conductivity of the fluid.

Firstly, the flow state of the cooling medium in the air gap should be determined by the Reynolds number. The determination formula is below [11]:

$$\begin{cases} \omega_r = \dfrac{\pi D_2 n_N}{60} \\ \omega_\delta = \sqrt{\left(0.5\omega_r\right)^2 + c_i^2} \\ R_e = \dfrac{\omega_\delta \delta}{v_r} \\ R_{ecr} = 41.2\sqrt{\dfrac{D_{i1}}{2\delta}} \end{cases} \tag{4}$$

where, R_e and R_{ecr} are the Reynolds number of the air gap and the key Reynolds number, respectively. For the Reynolds number of the air gap less than the rated Reynolds number, it indicates that the cooling medium in the air gap changes slowly. At this time, such a motion state is called laminar flow, and the equal thermal conductivity of the air gap equals to the thermal conductivity of the cooling medium. When the Reynolds number of the air gap is greater than the rated Reynolds number, it indicates that the cooling medium in the air gap changes drastically. At this time, such a state of motion is called turbulent flow. The equal thermal conductivity of the air gap is calculated according to formula (5) [12]:

$$\lambda_{eff} = 0.23\beta\left(\frac{2\delta}{D_2}\right)^{0.25} R_e^{0.5}\lambda_k \tag{5}$$

The interior space of the motor cavity researched herein is closed. After calculation, R_e = 559.8 < R_{ecr} = 860.0, and the equal thermal conductivity of the air gap is 0.0305$W\cdot m^{-1}\cdot K^{-1}$.

D. Heat Source Distribution

At present, the motor iron loss mainly adopts Bertotti, G Yu's separation calculation model of motor core loss, which divides the motor stator core loss into hysteresis loss, eddy current loss and additional loss. The calculation expression is shown in formula (6).

$$P_{Fe} = k_h f B_m^{\alpha} + k_e f^2 B_m^2 + k_{exc} f^{1.5} B_m^{1.5} \tag{6}$$

Copper loss is an important part of the loss of LSHTPMSM. Since the frequency of the motor researched herein is 25 Hz, the calculation formula is shown in formula (7).

$$P_{Cu} = m I_m^2 R_m \tag{7}$$

The magnetic field generated by the permanent magnet in the air gap changes periodically in the stator teeth, and a large number of harmonic magnetic fields are introduced. This cogging effect will form a large induced eddy current in the permanent magnet, and the resulting eddy current loss can be shown by Equation (8).

$$P_{Eddy} = \int_v E \cdot J dV = \int_v \rho J^2 dV \tag{8}$$

According to the motor parameters, a simulation model is established in the electromagnetic simulation software to simulate the change of motor loss under rated operating conditions. Fig. 3~4 shows the main loss variation curve of the motor.

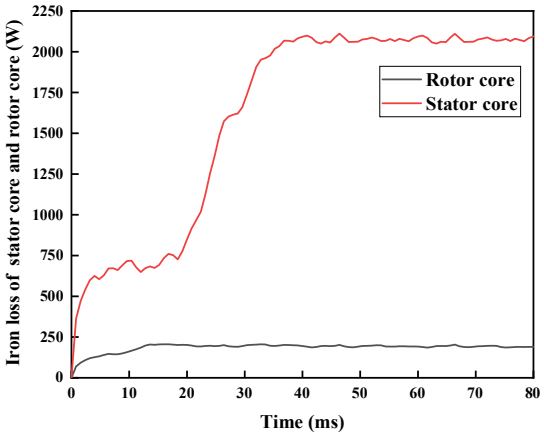

Fig. 3. Iron loss of motor stator core and rotor core

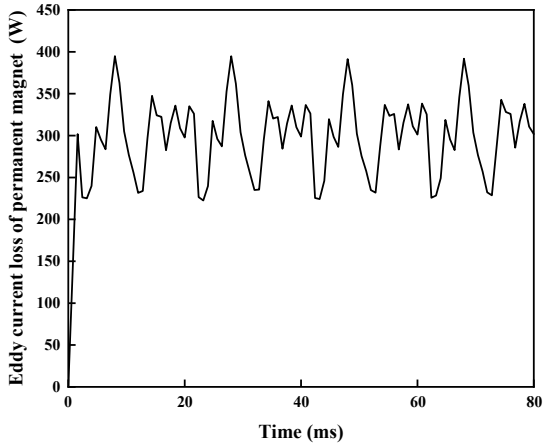

Fig. 4. Motor permanent magnet eddy current loss.

The motor will generate various losses under rated operating conditions, mainly in the form of heat. When simulating the temperature field of the motor, the heat production rate of every part of the motor shall be calculated, and it shall be applied to the corresponding heat generating elements. Table III shows the

heat production rate of the major heat-producing components in the motor.

This paper assesses that the thermal conductivity of every, and table IV shows the thermal conductivity of every material of the motor.

TABLE III
LOSS AND HEAT PRODUCTION RATE OF EVERY PART OF THE MOTOR

Electric machine parts	Loss (W)	Heat production rate($W \cdot m^{-3}$)
Stator core	2149.6	23681.3
Stator winding	18193.6	650172.7
Rotor core	227.1	204.3
Permanent magnet	353.9	6182.1

TABLE IV
THERMAL CONDUCTIVITY OF MOTOR MATERIALS

Electric machine parts	Thermal conductivity($W \cdot m^{-1} \cdot K^{-1}$)		
	X-direction	Y-direction	Z-direction
Stator core	39	39	4.43
Shell waterway	39.2	39.2	39.2
Stator winding	385	385	385
Winding equivalent insulation	0.29	0.29	0.29
Permanent magnet	9	9	9
Rotor core	39	39	4.43
Slot wedge	0.23	0.23	0.23
Air	0.0305	0.0305	0.0305

III. CALCULATION AND ANALYSIS OF MOTOR TEMPERATURE FIELD

Considering that the model of LSHTPMSM studied in this paper is large, it needs to occupy huge computer resources, and the calculation period is long, so the solution area can be reduced. Due to symmetrical motor in the axial direction, in order to decrease the amount of calculation, the axial half of the whole machine model and the radial one-twelfth are taken as the solution area. The model is imported into the simulation software, and the temperature field change of the motor under the rated situation is simulated according to the previous part. The simulation results are shown in Fig. 5-6.

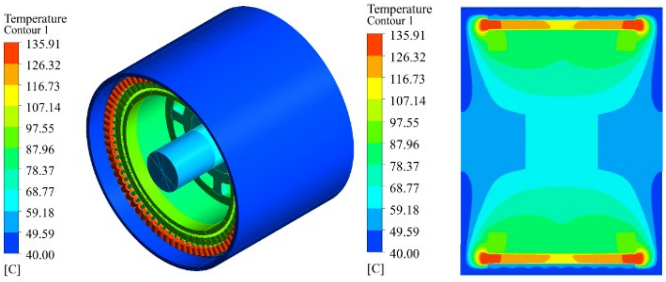

Fig. 5. Three dimensional temperature distribution and cross section of motor. (a) Three-dimensional temperature distribution. (b) Sectional drawing

From Fig. 5 (a) and (b), the temperature distribution of every part of the motor is relatively unified. The highest temperature part of the motor is located at the end of the stator winding, reaching 135.9 °C, and the lowest temperature part is located on the surface of the casing.

According to Fig. 6 (b), the stator winding shows a low middle and high end distribution under normal working conditions. The end winding shows significantly higher temperature than the winding in the slot. The most temperature rise of the winding reaches 95.9 K, and the temperature diversity with the winding in the slot reaches 20K. The average temperature rise reaches 82.6 K. This is because the end winding mainly relies on air convection heat dissipation, and the motor studied herein is a closed motor, the air velocity in the machine cavity is slow, the convection heat dissipation coefficient is small, resulting in heat accumulation, which is not conducive to heat dissipation, so the end winding has much higher temperature than the winding in the slot.

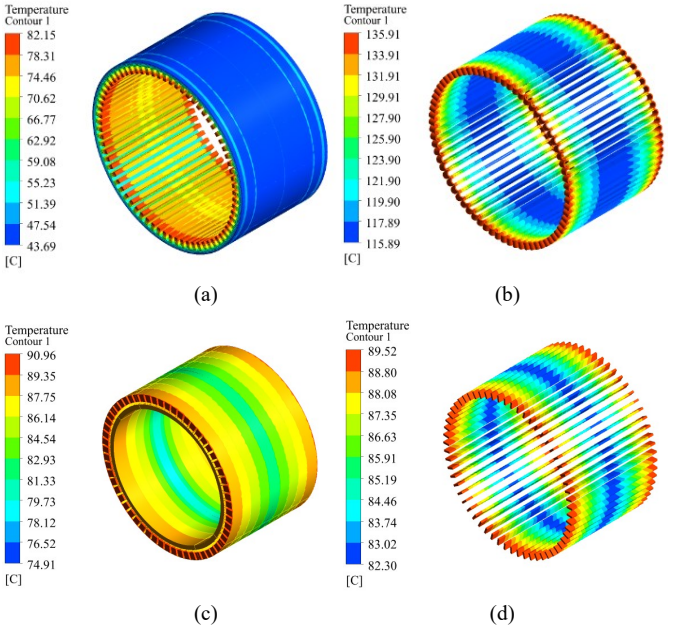

Fig. 6. Temperature distribution of motor parts. (a) Stator core. (b) Stator winding. (c) Rotor core. (d) Permanent magnet.

According to Fig. 6 (a), (c) and (d), the highest temperature of stator core, rotor core and permanent magnet is located at both ends, and the axial direction decreases to the middle, and the distribution is more uniform. The heat produced by the stator core is mainly cooled by heat transfer to the casing, so the radial temperature changes greatly; the heat produced by the rotor core and permanent magnet is mostly dissipated by convection with the air in the cavity, and the cooling conditions are limited.

Fig. 7 shows LSHTPMSM test platform. The temperature of the permanent magnet synchronous motor of low speed and high torque was tested under rated conditions.

Fig. 7. Prototype temperature rise experimental platform.

Because the temperature increase of the stator core winding of the LSHTPMSM is the most serious, the stator core winding is used as the test object of this experiment. Ten PT100 temperature sensors were embedded on the upper and lower sides of the stator core winding, respectively, to test and collect the temperature increase changes of the motor stator core winding under rated conditions. The comparison between the calculated results and the experimental data is shown in Table V.

TABLE V
COMPARISON OF CALCULATED OUTCOMES AND EXPERIMENTAL INFORMATION OF MOTOR WINDING TEMPERATURE FIELD

Type	Calculated value(K)	Experimental value(K)	Error (%)
Mean temperature rise	82.6	79.0	4.56
Maximum scale temperature-rise	95.9	92.1	4.23

It can be seen from the comparison results that the calculation results of the temperature field simulated by the software are more accurate and within the allowable error range. Under the rated operating condition, the stator core winding of the motor shows still too high temperature by using the cooling method of the casing water cooling, and the insulation requirements are high, which is not conducive to the long-term stable operation of the motor. Hence, the heat dissipation of the stator core winding shall be optimized.

IV. THERMAL CONDUCTION OPTIMIZATION ANALYSIS OF MOTOR END WINDING

A. Thermal Conductivity Optimization Design of End Winding

The end of the stator core winding contacts the air in the machine cavity, and the air thermal conductivity is low and the thermal conductivity is poor, so the heat generated by the stator core end winding cannot be effectively dissipated. For reducing the temperature increase of the end winding and the temperature diversity between the stator end winding and the slot winding, the insulation material with high thermal conductivity is filled at the end of the stator core winding to enhance the heat dissipation capacity of the end winding, thereby reducing the maximum temperature rise of the motor and improving the efficiency of the motor.

The calculation model of the three-dimensional heat transfer temperature field of the motor is built as shown in Fig. 8. The air with poor thermal conductivity around the end of the winding is filled with 140 MT epoxy thermal conductive sealant with good thermal conductivity, as shown in the black part of Fig. 8. Table VI displays the major thermal parameters. Fig. 9-10 shows the simulation outcomes.

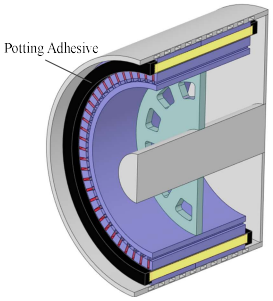

(a)

(b)

Fig. 8. Optimized motor model. (a)Three- dimensional heat transfer model of optimized motor. (b)Optimized motor stator end physical diagram.

TABLE VI
PARAMETERS OF 140 MT EPOXY HEAT CONDUCTIVE POTTING ADHESIVE

Parameter	Numerical value
Thermal conductivity($W \cdot m^{-1} \cdot K^{-1}$)	2.12
Density($kg \cdot m^{-3}$)	1300

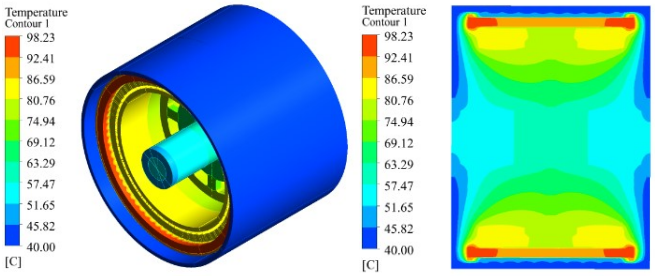

(a) (b)

Fig. 9. Three dimensional temperature distribution and cross section of optimized motor. (a) Three-dimensional temperature distribution. (b) Sectional drawing.

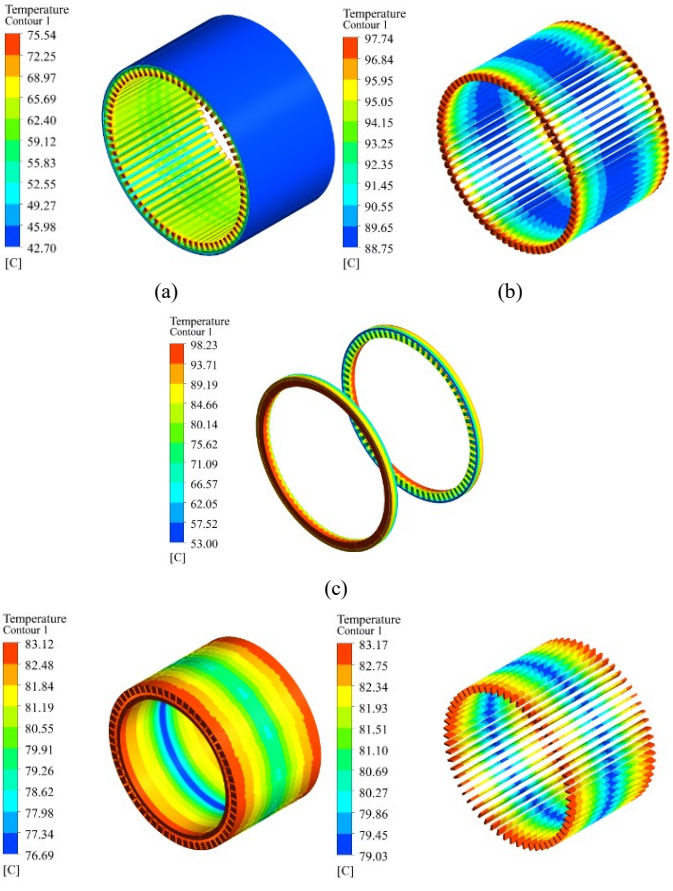

(a) (b) (c) (d) (e)

Fig. 10. Temperature distribution of optimized motor parts. (a) Stator core. (b) Stator winding. (c) Stator end potting adhesive. (d) Rotor core. (e) Permanent magnet.

According to the calculation outcomes in Fig. 9, the total temperature of the motor is effectively reduced after the heat conduction optimization at the end of the stator core winding. The most temperature increase at the end of the winding is decreased to 57.7 K, which is 37.8 K lower than that before optimization. The least temperature rise of the winding in the slot is reduced to 48.8K, and the temperature difference with the end winding is decreased to 9 K. The temperature increase of the permanent magnet is 5 K lower than that before optimization, and the temperature of the stator core and the rotor core is also slightly reduced. The overall temperature decrease of the motor is obviously improved after the optimization of the heat conduction at the end of the stator core winding, which is beneficial to improve the practical efficiency and service life of the motor.

B. Optimization Analysis of End Winding Heat Conduction

The axial length and radial width of the motor end potting adhesive are optimized, as shown in Fig. 11-12.

According to the image, with the increase of the axial length of the potting adhesive and the growth of the radial width, the temperature of the motor stator winding end declines. After comprehensive analysis, the potting adhesive with an axial length of 64 mm and a radial width of 86 mm is selected as the optimal parameter.

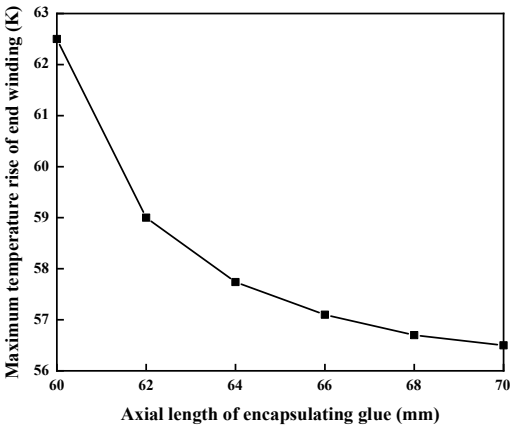

Fig. 11. Curve of maximum temperature of end winding with axial length of potting adhesive.

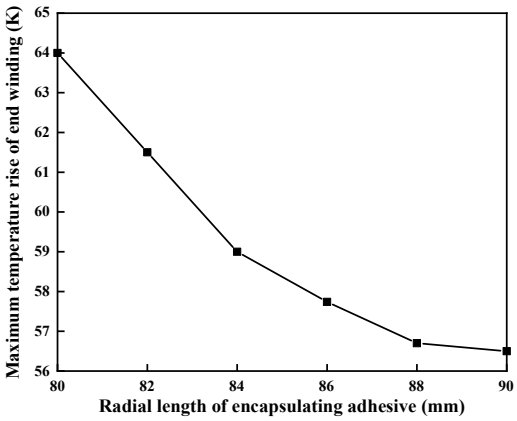

Fig. 12. Curve of maximum temperature of end winding with radial length of potting adhesive.

C. Experimental Verification

The temperature increase test platform of the optimized motor is built, and the temperature of the LSHTPMSM after the thermal conductivity optimization of the stator core winding end is tested under the same rated condition. The experimental value of the motor winding temperature is measured by the test platform. Table VII lists the calculation outcomes of the motor stator core winding and the experimental data comparison.

Table VIII lists the temperature comparison of the motor winding before and after optimization. The heat dissipation effect of the motor is improved by optimizing the heat conduction at the end of the stator winding, especially the heat dissipation role of the stator core winding.

TABLE VII
COMPARISON OF CALCULATION RESULTS AND EXPERIMENTAL DATA OF MOTOR WINDING TEMPERATURE FIELD AFTER OPTIMIZATION

Type	Calculated value	Experimental value	Error (%)
Mean temperature rise(K)	51.7	47.3	8.51
Maximum scale temperature-rise(K)	57.7	54.3	6.26

TABLE VIII
COMPARISON OF MOTOR WINDING TEMPERATURE RISE RESULTS BEFORE AND AFTER OPTIMIZATION

Type	Before optimization	After optimization	Temperature rise reduction ratio (%)
Mean temperature Rise (K)	82.6	51.7	-37.4
Maximum scale temperature-rise(K)	95.7	57.7	-39.8

V. CONCLUSION

This paper studies and analyzes the temperature field of LSHTPMSM. Firstly, a three-dimensional equivalent heat transfer temperature field calculation model is set up based on the physical model of the motor studied. The inner part of the stator core slot of the motor is equivalently processed, and the correctness of the three-dimensional equivalent heat transfer model is proved by experiments. Then, aiming at the problem that the water-cooling system of this type of motor will lead to serious heating of the stator winding end of the motor and large temperature difference between the stator winding end and the winding in the slot, the problem is optimized. By pouring sealant at both ends of the stator to replace the air with poor heat dissipation before, the temperature rise at the end of the stator core winding and the temperature difference between the end of the stator core winding and the winding in the stator core slot are effectively reduced, and the service life of the motor is improved. The final calculation outcomes display that the average temperature rise of the stator core winding of the motor is decreased from 82.6 K to 51.7 K, which is reduced by 37.4 %. The maximum temperature rise decreased from 95.9 K to 57.7 K, which was reduced by 39.8 %. The feasibility of the optimization scheme was validated by experiments, which provided a reference direction for the heat dissipation optimization of the permanent magnet synchronous motors of low speed and high torque with similar cooling conditions.

REFERENCES

[1] Y. D. Liu, “Review of Research on Low-speed and High-torque

Permanent Magnet Synchronous Motor," *Micromotors,* vol. 55, no. 4, pp. 77-81+93. Apr. 2022.
[2] X. Long, C. Y. Luo, and Z. M. Lu *et al*, "Thermal Analysis and Improvement of Slotless Tubular Permanent Magnet Linear Actuators Considering the Mechanical Air Gap," *Proceedings of the CSEE*, vol. 39, no. 7, Apr. 2019.
[3] C. Sciascera, P. Giangrande, and L Papini *et al*, "Analytical Thermal Model for Fast Stator Winding Temperature Prediction," *IEEE Tranasctions on Industrial Electronics,* vol. 64, no. 8, pp. 6116-6126. Aug. 2017.
[4] L. Chen, Y. Sun, and J. L. Fang *et al*, "Calculation of Temperature Rise for Permanent Magnet Hub Motor under Overload Condition," *Journal of Electrical Engineering,* vol. 14, no. 1. pp. 9-14, Mar. 2019.
[5] L. Y. Li, J. P. Zhang, and H. Y. Yan *et al*, "Study on the Optimization of Thermal Conductivity and 3D Temperature Filed Calculation for the High Power Density Motor," *Proceedings of the CSEE,* vol. 36, no. 13, pp. 3642-3650, Jul. 2016.
[6] J. Zhang, Z. R. Zhang, and Y. W. Xia *et al*, "Thermal Analysis and Management for Doubly Salient Brushless DC Generator with Flat Wire Winding," *IEEE Transactions on Energy Conversion,* vol. 35, no. 2, pp. 1110-1119, Dec. 2020.
[7] J. Zhang, Z. R. Zhang, and Y. Li, "Thermal Deformation Analysis of Water Cooling Doubly Salient Brushless DC Generator with Stator Field Winding," *IEEE Transactions on Energy Conversion,* vol. 67, no. 4, pp. 2700-2710, Apr.2017.
[8] S. K. Zhang, W. L. Li, and J. Y. Li *et al*, "Research on Flow Rule and Thermal Dissipation Between the Rotor Poles of a Fully Air-cooled Hydrogenerator," *IEEE Transactions on Industrial Electronics,* vol. 62, no. 6, pp. 3430-3437, Jun. 2015.
[9] W. L. Li, J. Y. Li, and D. Li, "Influence of Variable Section Rotor Ventilation Ducts on Temperature and Fluid Fields of a Full Air-cooled Large Hdro-generator Rotor" *Transactions of China Electrotechnical Society*, vol. 32, sup.2, pp. 42-49, Oct. 2017.
[10] X. G. Fan, R. H. Qu, and J Li *et al*, "Ventilation and Thermal Improvement of Radial Forced Air-cooled FSCW Permanent Magnet Synchronous Wind Generators," *IEEE Transactions on Industry Applications,* vol. 53, no. 4, pp. 3447-3456, Jul. 2017.
[11] W. M. Tong, X. B. Cheng, and J. Y. Sun *et al*, "Suppression Effect of Rotor Wafters on Permanent Magnet Temperature Rise for High-speed Permanent Magnet Motor," *Proceedings of the CSEE*, vol. 37, no. 5, pp. 1526-1534, Mar. 2017.
[12] M. Cheng, S. Ding, and W. Li *et al*, "Cooling System Design and Thermal analysis of a PMSM for Rail Transit," in Proc. of *2020 15th IEEE Conference on Industrial Electronics and Applications (ICIEA)*, Kristiansand, Norway, pp. 1912-1915, 2020.
[13] X. Y. Wang, and P. Gao, "Analysis of 3-D Temperature Field of In-wheel Motor with Inner-oil Cooling for Electric Vehicle," *Electric Machines and Control,* vol. 20, no. 3, pp. 36-42, Mar.2016.

Shengnan Wu (M'18) was born in Yingkou, China. She received the B.S., M.S., and Ph.D. degrees in electrical engineering from the Shenyang University of Technology, Shenyang, China, in 2008, 2011, and 2017, respectively.

She is currently a Postdoctoral Research Assistant in electrical engineering with Shenyang University of Technology. Her research interests include electromagnetic design and multiphysical field simulation and analysis of permanent magnet machines.

Zhimin Li was born in Shanxi, China. He received his bachelor's degree in electrical engineering from Shenyang University of technology in Shenyang, China in 2020. Currently, he is studying for a master's degree in electrical engineering at Shenyang University of technology in China.

His main research interests include cooling system design and thermal calculation of low speed high torque permanent magnet synchronous motor.

Wenming Tong (M'18) was born in Dandong, China. He received the B.S. and Ph.D. degrees in electrical engineering from the Shenyang University of Technology, Shenyang, China, in 2007 and 2012, respectively. He is currently an Associate Professor with the National Engineering Research Center for Rare Earth Permanent Magnet Machines, Shenyang University of Technology.

His major research interests include the design, analysis, and control of high-speed and low-speed direct drive permanent magnet machines, axial flux permanent magnet machines, hybrid excitation machines, and high-performance machines with new types of soft magnetic materials.